Article

The Role of a Simple Inerter in Seismic Base Isolation

R.S. Jangid *

Posted Date: 15 December 2023

doi: 10.20944/preprints202312.1127.v1

Keywords: floor accelerations; fluid inerter damper; real earthquake; seismic base isolation; stationary excitation; tuned mass damper-inerter

Article

The Role of a Simple Inerter in Seismic Base Isolation

R.S. Jangid *

Department of Civil Engineering, Indian Institute of Technology Bombay, Powai, Mumbai - 400 076 (India)
* Correspondence: emai: rsjangid@civil.iitb.ac.in; ORCID: https://orcid.org/0000-0002-2408-2368

Abstract: The present study investigates the role of a simple inerter in supplemental devices for possible implementation in the matured seismic base isolation technique. Firstly, the response of the base-isolated structure with an optimally tuned mass damper-inerter (TMDI) is investigated to see the tuning effects. The time required to tune the TMDI was found to be significantly longer than the duration of a strong-motion earthquake. There was still a reduction in the response of the isolated structure, which is primarily due to the added damping and stiffness (ADAS) of TMDI and not because of the tuning effects. Hence, it is proposed that the corresponding ADAS of the TMDI be directly added to the isolation device. Secondly, the response of the base-isolated structures with the fluid inerter damper (FID) is studied. It was observed that the inerter of the FID does not influence the displacement variance of an isolated structure under broadband earthquake excitation. It implies that the response of the isolated structure with FID is primarily controlled by its counterpart fluid damper (FD). The performance of optimal TMDI, ADAS, FID, and FD to mitigate the seismic response of the flexible multi-story base-isolated structure under real earthquake excitations is also investigated. In terms of suppressing the displacement and acceleration responses of the isolated structure, it has been found that TMDI and ADAS perform similarly. Comparing the response of the isolated structure with FID and FD demonstrated that the inerter in the FID has detrimental effects on the isolated structures, in which the top floor's acceleration and base shear are substantially increased.

Keywords: floor accelerations; fluid inerter damper; real earthquake; seismic base isolation; stationary excitation; tuned mass damper-inerter

1. Introduction

Inerter-based dampers have recently seen tremendous growth in popularity for controlling structural vibration [1]. Inerter is used for the mass enhancement effects, and its resisting force is predicted to be proportional to the relative acceleration between ends [2]. A tuned mass damper-inerter (TMDI) simulates a conventional tuned mass damper (TMD) with an inerter. Additionally, it is referred to as a tuned inerter damper (TID) when the TMD mass is replaced with the inerter. The performance of base-isolated structures with TMDI fixed to the isolation floor under both real and stochastic earthquake excitation was examined [3–13]. It was demonstrated that the TMDI reduces the response of base-isolated structures equipped with linear as well as non-linear isolators. Enhanced performance of the optimal TMDI was further observed when it was placed on the upper floors of the isolated structure or used in tandem [14,15]. Recently, it has also been demonstrated experimentally that it is possible to achieve reasonable results in the response of base-isolated structures augmented with TMDI by using a simplified linear dissipative model instead of a nonlinear model with friction and gear backlash [16,17]. The efficiency and optimum TID parameters for the base-isolated structure when considering the stochastic model of earthquake excitation are also illustrated [18–23]. To reduce the seismic response and vibration isolation in the base-isolated structures, a geometrically nonlinear TID arrangement is also being investigated for multidirectional isolation [24]. The use of multiple TMD to control the seismic response of base-isolated buildings has recently been studied [25,26]. Another application of the inerter in seismic base isolation was the supplemental fluid inerter damper (FID) and electromagnetic inertial mass damper (EIMD). The performance of the base-isolated structures with FID has been investigated by various researchers

 doi:10.20944/preprints202312.1127.v1

and has shown that there are benefits in seismic response control [27–34]. Recently, the dynamic behaviour of EIMD and optimal parameters for reducing the structural response of base-isolated structures were also demonstrated [35,36]. The review above suggests that the researchers are very interested in using inerter-based supplemental devices for base-isolated structures.

The period of base-isolated structures is usually quite long, and the tuning effects of TMDI, TID, or TMD may not be achieved during the strong motion duration of the earthquake excitation. However, there is still a reduction in the response of the isolated structure, which is primarily due to the added damping and stiffness (ADAS) of the above devices and not because of the tuning effects [37]. The tuned damper-type devices are relatively less effective for the system with higher damping than the corresponding systems with lower damping [38]. It implies that for base-isolated buildings generally equipped with heavy damping, the supplemental tuned mass-type damper devices may not be very effective. Further, in the FID and EIMD, the inerter works in tandem with the fluid damper (FD) and electromagnetic damper (ED), and it's unclear whether the inerter or the FD and ED provide beneficial effects in response reduction. It may be possible that a single FD or ED can achieve similar or even better beneficial effects. As a result, it will be interesting to investigate the controlling effects of the inerter by examining the seismic response of base-isolated structures with FID or EIMD. This is proposed to be achieved by comparing the response of isolated structures with FID or EIMD with the corresponding response without inerter in the FID or EIMD devices.

Herein, the response of the base-isolated structures with supplemental optimal TMDI and FID is investigated for the tuning effects of TMDI and the role of inerter in FID. The specific objectives of the study are summarized to (i) investigate the tuning effects of TMDI in controlling the seismic response of the base-isolated structure equipped with TMDI, (ii) compare the response of base-isolated structures with TMDI to the corresponding response with ADAS device, (iii) understand the role of inerter in FID for seismic response control of base-isolated structure by comparing the corresponding response with FD, and (iv) to study the comparative performance of TMDI, ADAS, FID, and FD devices for flexible multi-story base-isolated structures subjected to real earthquakes.

2. Base-Isolated Rigid Structure with TMDI and ADAS

The multi-story building model in Figure 1a is thought of as having a rigid superstructure, base isolation, and TMDI or ADAS. The base mass and the superstructure's combined mass are represented by the mass m. The equivalent linear force-deformation behaviour with viscous damping, which is specific to the building, defines the isolation system. Let k_b and c_b represent the equivalent stiffness and damping of the selected isolation system, respectively. Two parameters, namely, isolation period T_b and damping ratio ξ_b, are used to characterize the base isolation system under consideration and are expressed as

$$T_b = \frac{2\pi}{\omega_b}, \quad \omega_b = \sqrt{\frac{k_b}{m}} \quad \text{and} \quad 2\xi_b\omega_b = \frac{c_b}{m} \tag{1}$$

Preprints (www.preprints.org) | NOT PEER-REVIEWED | Posted: 15 December 2023 doi:10.20944/preprints202312.1127.v1

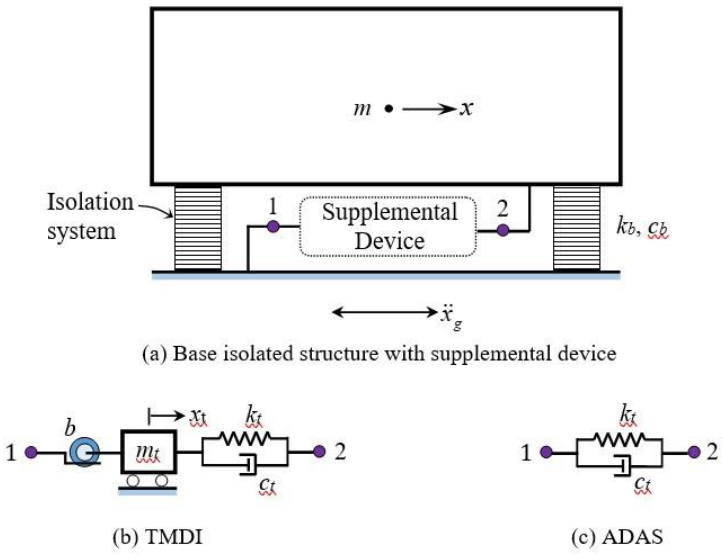

Figure 1. Idealization of the rigid superstructure of the multi-story building with base isolation and supplemental devices.

3.1. Supplemental TMDI Device

The TMDI device consists of an auxiliary mass (m_t), stiffness (k_t), and damper (c_t) referred to as TMD, and an inertial device with an inertance coefficient as b (refer to Figure 1b). The two terminals of the inertial device are connected to the auxiliary mass and the ground. A reaction force is generated by the inertial device's motion that, roughly speaking, can be regarded as proportional to the relative acceleration developed between the two terminals. The inertance, also known as apparent mass, is a proportional coefficient that can be numerous times the inerter's actual mass. The energy is dissipated through damping when the resonance in the TMD is introduced together by the vibration of the base-isolated structure. The modeling aspects of the TMDI for practical usage had been confirmed through the experimental study of the dynamic response of an isolated structure system equipped with TMDI tested on shaking table [16,17]. Also, TMDI is observed to be robust when a change of the design parameters from their optimal values does not produce significant response variations [39]. The auxiliary and inertial masses coupled to the TMDI are represented by the mass and inertance ratio defined as

$$\mu = \frac{m_t}{m} \quad \text{and} \quad \beta = \frac{b}{m} \tag{2}$$

The TMDI's corresponding stiffness and damping are expressed as

$$\xi_t = \frac{c_t}{2(m_t+b)\omega_t}, \quad \omega_t = \sqrt{\frac{k_t}{m_t+b}} \quad \text{and} \quad f = \frac{\omega_t}{\omega_b} \tag{3}$$

where ξ_t and f represent the damping ratio of the TMDI and tuning frequency ratio, respectively.

The equations governing the motion of the building model with a rigid superstructure, base isolation, and TMDI are represented by

$$\begin{bmatrix} m & 0 \\ 0 & m_t + b \end{bmatrix} \begin{Bmatrix} \ddot{x} \\ \ddot{x}_t \end{Bmatrix} + \begin{bmatrix} c_b + c_t & -c_t \\ -c_t & c_t \end{bmatrix} \begin{Bmatrix} \dot{x} \\ \dot{x}_t \end{Bmatrix} + \begin{bmatrix} k_b + k_t & -k_t \\ -k_t & k_t \end{bmatrix} \begin{Bmatrix} x \\ x_t \end{Bmatrix} = -\begin{Bmatrix} m \\ m_t \end{Bmatrix} (\ddot{x}_g) \tag{4}$$

where x = relative displacement of the isolated structure; x_t = relative displacement of the auxiliary mass of the TMDI; and $\ddot{x}_g$= earthquake acceleration.

Let the earthquake acceleration be harmonic as $\ddot{x}_g = e^{j\omega t}$, where ω is the circular frequency and $j = \sqrt{-1}$, the steady-state displacement x is expressed as

Preprints (www.preprints.org) | NOT PEER-REVIEWED | Posted: 15 December 2023 doi:10.20944/preprints202312.1127.v1

$$x = H_x(j\omega)\ e^{j\omega t} \tag{5}$$

where $H_x(j\omega)$ = frequency response function (FRF) of the displacement x.

The SDOF model of the base-isolated structure with TMDI is subjected to white-noise earthquake acceleration with the power spectral density function (PSDF) as S_0. The mean square displacement of the isolated structure can be expressed as

$$\sigma_x^2 = \int_{-\infty}^{\infty} |H_x(j\omega)|^2\ S_0\ d\omega \tag{6}$$

By dividing the corresponding response from the base-isolated structure with no control, the mean square response obtained from equation (6) is further normalized i.e.

$$\tilde{\sigma}_x^2 = \frac{\sigma_x^2}{\sigma_{x,0}^2} \quad \text{and} \quad \sigma_{x,0}^2 = \frac{\pi S_0}{2\xi_b \omega_b^3} \tag{7}$$

The TMDI system is effective at response mitigation if the normalized variance, $\tilde{\sigma}_x^2$ value is less than unity.

The parameters μ, β, ξ_t, and f provide a complete description of the supplemental TMDI for the base-isolated structure. For all numerical solutions in the current study, μ is taken to be equal to 0.01 because the TMDI performs best for a smaller value of μ and higher values of β [39]. It is also worth mentioning that when μ = 0, the TMDI is reduced to the TID. When ξ_t and f are set to their optimum values, the TMDI performs at its best. For a given base-isolated structure (i.e., specified by T_b and ξ_b) and white-noise earthquake excitation, the optimum parameters of the TMDI (i.e., optimum ξ_t and f) are the ones that minimize the σ_x^2. This is referred to as 'optimal TMDI' in the present study throughout and the corresponding optimum ξ_t and f are obtained using an algorithmic numerical search technique for values spanning their feasible regions with increments of 0.0001. Using the above-specified procedure with isolation damping, ξ_b not exceeding 10 percent, the optimum damping ratio (ξ_t^{opt}) and tuning frequency ratio (f^{opt}) for a selected value of β can be calculated using the following expressions from [40]

$$\xi_t^{opt} = \sqrt{\frac{\beta(4+3\beta)}{8(1+\beta)(2+\beta)}} \tag{8}$$

$$f^{opt} = \frac{1}{1+\beta}\sqrt{\frac{(1+\frac{\beta}{2})}{(1+\xi_b)}} \tag{9}$$

The variation of the FRF of displacement of a base-isolated structure with optimal TMDI is plotted in Figure 2. The inertance ratio is considered to be 0.1, 0.2, and 0.4, and the FRF responses are compared with the corresponding base-isolated structure without TMDI (referred to as BIS). The FRF of isolated structures with optimal TMDI appears to be a two-peaked response. The optimization of parameters occurs when the response to the second peak is minimized. The maximum reduction in FRF occurs at the resonating frequency, and there is a reduction of 60.8, 68.1, and 75.1 percent for the inertance ratio of 0.1, 0.2, and 0.4, respectively. Thus, it can be concluded that the TMDI effectively reduces the FRF and, thereby, the mean square of the displacement response of the base-isolated structure.

It was observed in Figure 2 that the optimal TMDI mitigates the FRF of the base-isolated structure under resonating conditions. However, it will be interesting to know how much time or the number of cycles the TMDI needs to attain fully tuned conditions for maximum response reduction. To verify this, the displacement of the base-isolated structure with and without optimal TMDI subjected to earthquake acceleration of $\ddot{x}_g = sin(2\pi t/3)$ m/sec² (t denotes here the time in sec) is calculated using the numerical integration procedure and plotted in Figure 3. It is observed from the figure that after one cycle of response, the reduction of the displacement is 12.4, 27.7, and 39.1 percent for the inertance ratio of 0.1, 0.2, and 0.4, respectively. To achieve the maximum reduction in the

Preprints (www.preprints.org) | NOT PEER-REVIEWED | Posted: 15 December 2023 doi:10.20944/preprints202312.1127.v1

response under resonating conditions, the TMDI should undergo several cycles of responses (i.e., about 10 cycles as per Figure 3). Normally, such many cycles may not be possible during the strong motion duration of past recorded earthquakes. Despite that, there is a reduction in the response by the TMDI in the initial cycles, which is primarily attributed to the added heavy damping of its auxiliary damper. It is to be noted that the added damping by optimal TMDI is 0.16, 0.48, and 0.87 times the isolation damping for the inertance ratio of 0.1, 0.2, and 0.4, respectively.

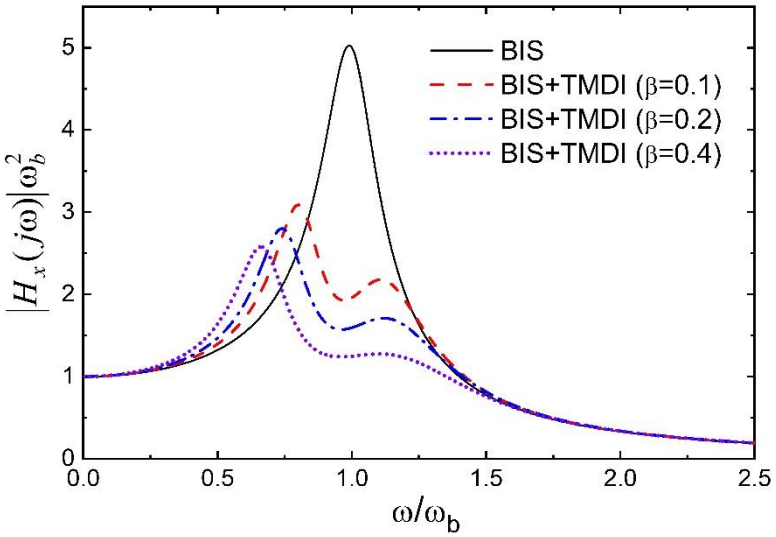

Figure 2. Variation of FRF of displacement of base-isolated structure with optimal TMDI (T_b = 3 sec and ξ_b = 0.1).

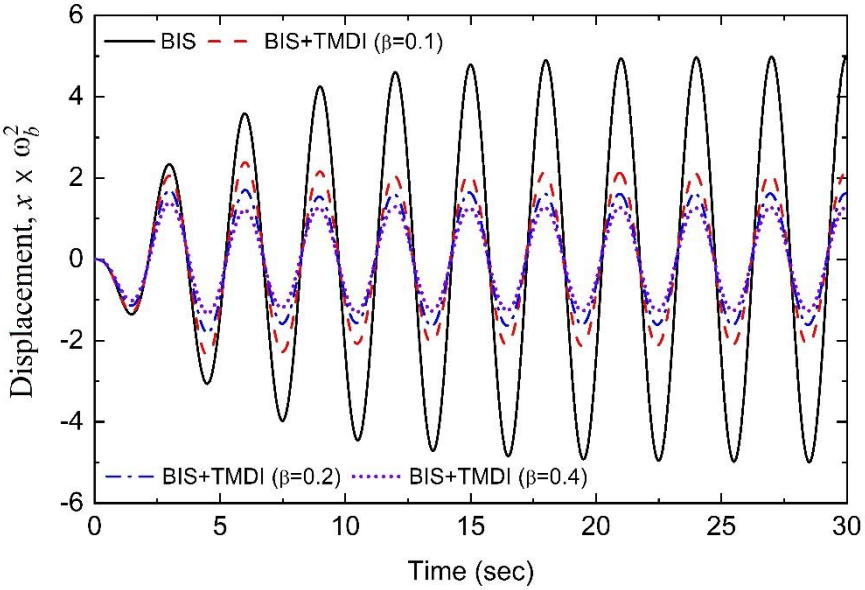

Figure 3. Time variation of displacement of base-isolated structure with optimal TMDI under harmonic excitation (T_b = 3 sec and ξ_b = 0.1).

3.2. Supplemental ADAS Device

Figure 3 showed that the ADAS is responsible for the decrease in displacement of the base-isolated structure with optimal TMDI in the first cycles [37]. It is to be further noted that TMDI in base-isolated structures will be ineffective when subjected to near-fault pulse-type earthquake ground motions [41]. Under this condition, the response of the isolated structure is governed by the pulses associated with the earthquake record, and the tuning effects of TMDI will be unachievable. In view of the above facts, in place of the TMDI, it is proposed that the ADAS be added parallel to

Preprints (www.preprints.org) | NOT PEER-REVIEWED | Posted: 15 December 2023 doi:10.20944/preprints202312.1127.v1

the isolation system, which may provide better control (refer to Figure 1c). For a specified inertance, the corresponding stiffness (k_t), and damper (c_t) of the 'optimal TMDI' constitute the ADAS in the present study. This is merely a comparison; additional optimal ADAS exploration can be conducted to achieve the desired response control of the base-isolated structures.

A comparison of normalized displacement variance of the base-isolated structure with the optimal TMDI and corresponding ADAS is depicted in Figure 4. The plotting of the response is done for the damping ratio, ξ_b = 0.05, 0.1, 0.15, and 0.2, and the isolation period, T_b = 3 sec. The figure reveals that for the lower inertance ratios, the normalized variance of base-isolated with TMDI is lower than the corresponding ADAS. However, for the higher inertance ratio, the ADAS is superior to the TMDI in reducing the displacement variance of the base-isolated structure. This can be explained by the fact that while the TMDI's performance is unaffected by higher inertance ratios, the amount of auxiliary damping (i.e., c_t) needed to achieve the best results is higher [40]. The performance of the isolated structure in displacement reduction improves when this damper with the high damping as ADAS is attached directly to the ground and isolation floor. This figure also indicates that the reduction in displacement by the TMDI is more significant for isolated structures with lower damping in comparison to higher damping and confirms the recent finding [40].

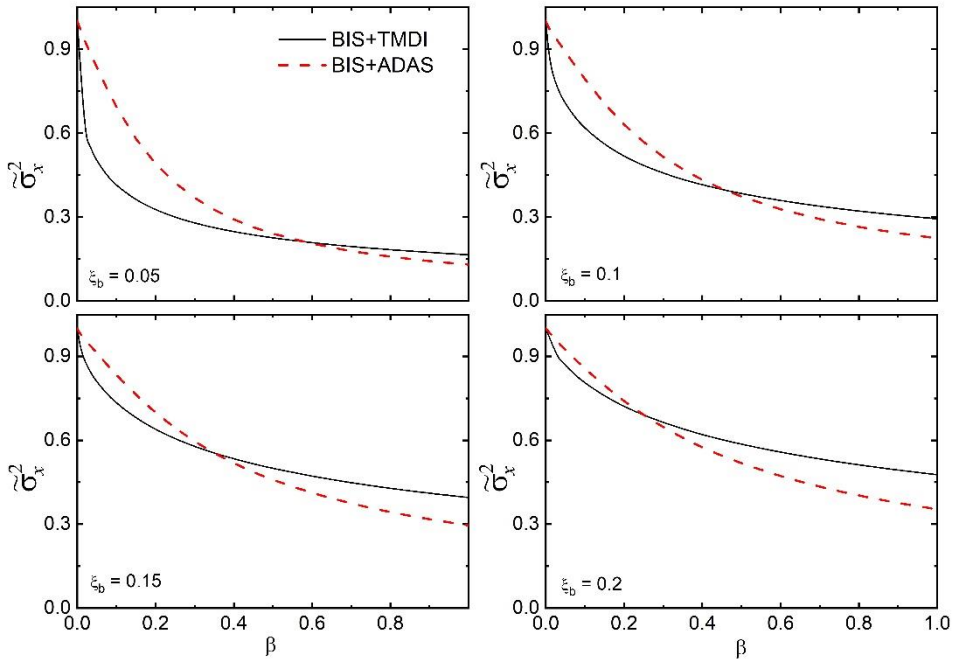

Figure 4. The plot of normalized displacement variance of base-isolated structure with optimal TMDI and corresponding ADAS against the inertance ratio.

3. Rigid Base-Isolated Structure with FID and FD

Figure 5a depicts a schematic diagram of FID installed in a rigid model of the base-isolated structure. The two terminals, represented by 1 and 2 on the FID, are coupled to the ends depicted in Figure 1a of the base-isolated structure model. An FID typically consists of a piston and cylinder that force the fluid through a helical tube that is encircled by the cylinder. The hydraulic cylinder and the piston rod are the two terminals of the FID. The fluid flow through an external helical channel produces rotational inertia to compensate for the pressure loss [42–44]. The FID's resisting force depends on the friction, oil density, and viscosity of the fluid. The FID is modelled as a linear inerter in parallel with a linear [27–29,32,33] and a non-linear [30,31] dashpot for studying the seismic response of the base-isolated structures. For simplicity, the FID is modelled in the present study as a linear inerter (i.e., with an inertance coefficient as b) in parallel with a linear viscous FD (i.e., with a damping coefficient of c_f). It is worth noting that this FID modelling is identical to the EIMD modelling described in the References [35,36].

Preprints (www.preprints.org) | NOT PEER-REVIEWED | Posted: 15 December 2023 doi:10.20944/preprints202312.1127.v1

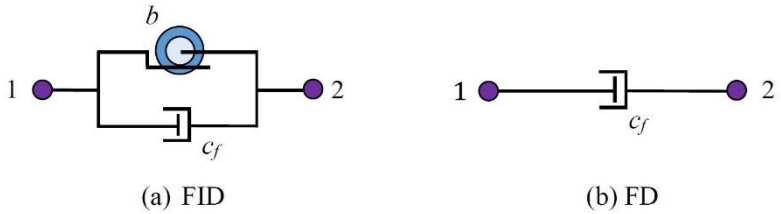

(a) FID (b) FD

Figure 5. Schematic diagram of supplemental FID and FD devices.

The FID is defined by two parameters, β and ξ_f, which are both defined as:

$$\beta = \frac{b}{m} \text{ and } \xi_f = \frac{c_f}{2m\omega_b} \tag{10}$$

Consider the rigid superstructure model of the base-isolated structure (refer to Figure 1a) with supplemental FID. The governing equation of motion of a base-isolated structure with FID under earthquake excitation is expressed as

$$(m+b)\ddot{x} + (c_b + c_f)\dot{x} + k_b x = -m\ddot{x}_g \tag{11}$$

Dividing equation (11) by (*m*+*b*) and substituting $\beta = b/m$, the equation of motion reduces to

$$\ddot{x} + 2\left(\frac{\xi_b + \xi_f}{\sqrt{1+\beta}}\right)\left(\frac{\omega_b}{\sqrt{1+\beta}}\right)\dot{x} + \left(\frac{\omega_b}{\sqrt{1+\beta}}\right)^2 x = -\left(\frac{1}{1+\beta}\right)\ddot{x}_g \tag{12}$$

The above indicates that FID elongates the vibration period and decreases the total damping ratio (i.e., $\xi_b + \xi_f$) of the base-isolated structure. It also suppresses the level of earthquake shaking (as the denominator on the right-hand side is always larger than unity).

Let the rigid superstructure model of the base-isolated structure with FID be subjected to white-noise earthquake acceleration with PSDF as S_0. The mean square displacement of the isolated structure with FID will be [45]

$$\sigma_x^2 = \frac{\pi S_0}{2(\xi_b + \xi_f)\omega_b^3} \tag{13}$$

The above equation indicates that for broadband excitation, the displacement variance of the base-isolated structure is not influenced by the inertance of the FID. The reduction in displacement is primarily happening due to the added damping of the FID. Since the inerter of the FID does not influence the response of the isolated structures under broad band-excitation, it is therefore proposed that the corresponding FD only be added parallel to the isolation system (refer to Figure 5b).

The absolute acceleration, $\ddot{x}_a$ of the isolated structural mass with FID, is expressed as

$$\ddot{x}_a = [\ddot{x} + \ddot{x}_g] = -[\omega_b^2 x + 2(\xi_b + \xi_f)\omega_b \dot{x} + \beta\ddot{x}] \tag{14}$$

Interestingly, two terms i.e., $2\xi_f\omega_b\dot{x}$ and $\beta\ddot{x}$ are added to the absolute acceleration of the mass compared to the conventional isolation system, and it will be interesting to see their effects.

When subjected to the harmonic earthquake acceleration as $\ddot{x}_g = e^{j\omega t}$, the steady-state absolute acceleration, $\ddot{x}_a$ is expressed as

$$\ddot{x}_a = H_{\ddot{x}_a}(j\omega)\, e^{j\omega t} \tag{15}$$

where $H_{\ddot{x}_a}(j\omega)$ is the FRF of the response $\ddot{x}_a$.

In Figure 6, the variation of the FRF of the absolute acceleration of the mass of the isolated structure with FID is plotted. The FRF with β = 0 corresponds to the structure without FID. Because of the added supplement inertial mass by the FID, the resonating frequency decreases as the inertance ratio increases. The peak values of absolute acceleration also decrease with the increase of the β. However, for higher frequencies, the amplitude of absolute acceleration increases with the β and remains constant throughout. This implies that FID will transmit earthquake vibrations into the base-isolated structures associated with the higher frequencies. This can be detrimental to the sensitive

Preprints (www.preprints.org) | NOT PEER-REVIEWED | Posted: 15 December 2023 doi:10.20944/preprints202312.1127.v1

high-frequency equipment or secondary system installed in the isolated structure. It is also to be noted that the mean square absolute acceleration of the isolated structure with FID, $\sigma^2_{\ddot{x}_a} \to \infty$ when subjected to white-noise earthquake excitation.

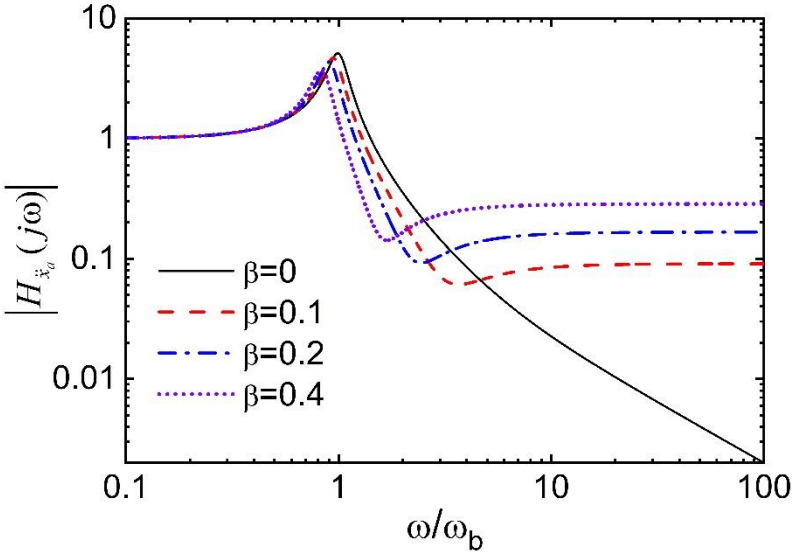

Figure 6. Variation of FRF of absolute acceleration of the mass of the isolated structure with FID (T_b = 3 sec, ξ_b = 0.1, and ξ_f = β/2).

4. Response Under Filtered White-Noise Excitation

Unpredictable and multi-dimensional ground motions are always present during earthquakes. If the frequency content evolution is disregarded, the stationary ground motion can be represented by a PSDF matrix. The PSDF of the earthquake excitation is considered as that suggested by Kanai and Tajimi [46,47] i.e.

$$S_{\ddot{x}_g}(\omega) = S_0 \left(\frac{1 + 4\xi_g^2(\omega/\omega_g)^2}{[1-(\omega/\omega_g)^2]^2 + 4\xi_g^2(\omega/\omega_g)^2} \right) \tag{16}$$

where $S_{\ddot{x}_g}(\omega)$ = PSDF of the earthquake acceleration $\ddot{x}_g$; ω_g = predominant frequency of the soil media or filter; and ξ_g = damping ratio of the soil media or filter. The values of filter parameters selected are ω_g = 15 rad/sec and ξ_g=0.6 which corresponds to a firm type of soil media.

A comparison of $\tilde{\sigma}_x^2$ of the base-isolated with optimal TMDI, ADAS, FID, and FD subjected to the Kanai-Tajimi model of earthquake excitation is shown in Figure 7. The responses are plotted for isolation period, T_b = 3 and 4 sec and damping ratio, ξ_b = 0.1. As observed earlier, the performance of the corresponding ADAS device is better than the TMDI for higher inertance ratios. The displacement variance of the base-isolated structure with FID and corresponding FD under filtered white-noise excitation also does not differ, as was also seen for the white-noise excitation

Preprints (www.preprints.org) | NOT PEER-REVIEWED | Posted: 15 December 2023 doi:10.20944/preprints202312.1127.v1

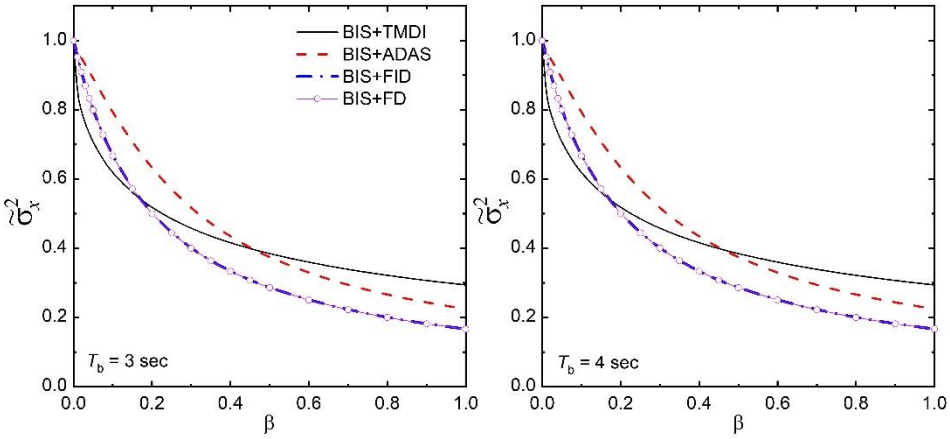

Figure 7. Comparison of normalized displacement variance of the base-isolated structure with optimal TMDI, ADAS, FID, and FD subjected to of Kanai-Tajimi model of earthquake excitation (ξ_f = β/2 and ξ_b = 0.1).

5. Flexible Isolated Structure Under Real Earthquakes

An earlier study attempted the response of a rigid base-isolated structure with the optimum TMDI, ADAS, FID, and FD under stationary earthquake excitation. However, the behaviour of these devices under real earthquake excitation and when the isolated superstructure is assumed to be flexible will be interesting to explore. This will provide insight into the tuning behaviour and the frequency contents of the superstructure acceleration of the isolated structure with TMDI and FID. Figure 8a depicts a typical five-story linear shear-type building equipped with supplementary TMDI, ADAS, FID, and FD devices in addition to a base isolation system. The base mass and the i^{th} floor mass are represented by m_b and m_i, respectively. k_i stands for the i^{th} floor's stiffness. The lead-rubber bearing (LRB) system is selected as an isolation device. Hysteretic damping is additionally produced by the lead core of the LRB through yielding, which dissipates the seismic energy input. Figure 8b illustrates the simple bi-linear force-deformation behaviour of the LRB. The three variables F_y, k_b, and q, which stand for yield force, post-yield stiffness, and yield displacement, respectively, define the LRB's bi-linear characteristics. For the selected base-isolated structure with supplemental TMDI, ADAS, FID, and FD, the governing equations of motion are

$$\mathbf{M}\ddot{\mathrm{x}}(t) + \mathbf{C}\dot{\mathrm{x}}(t) + \mathbf{K}\mathrm{x}(t) + \mathbf{D}_i F_i(t) + \mathbf{D}_s \mathbf{F_s}(t) = -\mathbf{E}\ddot{x}_g(t) \qquad (17)$$

where **M** = mass matrix; **C** = damping matrix; **K** = stiffness matrix; **x**(t) = vector of horizontal displacements (relative to the ground) of each mass at time t; $\mathbf{D_i}$ = location vector for the bi-linear restoring force of the LRB; $F_i(t)$ = bi-linear restoring force of the LRB; $\mathbf{D_s}$ = location matrix for the vector of control forces $\mathbf{F_s}(t)$ produced by the supplemental devices TMDI, ADAS, FID, and FD; **E** = vector containing the vibrating masses; and $\ddot{x}_g(t)$ = earthquake acceleration specified by a time history.

A five-story building with linear inter-story stiffness and viscous damping is selected for the present study, and its parameters are taken from Kelly [48]. All floors and base raft locations in the selected superstructure account for the same mass implying $m_b = m_i$ (i=1 to 5). The inter-story stiffness of various floors is taken as k_1, k_2, k_3, k_4, and k_5, which correspond to, respectively, 15k, 14k, 12k, 9k, and 5k. The chosen value for k results in a fundamental period of 0.4 seconds for the fixed base-superstructure. The superstructure with a fixed base has five natural frequencies that are measured in rad/sec and are 15.71, 38.48, 60.84, 83.12, and 105.37. Assuming that all vibrational modes have a modal damping ratio of 0.02, the superstructure's damping matrix is developed. The parameters T_b and ξ_b (see equation (1)) are used to calculate the post-yield stiffness and damping of the LRB while considering the flexible base-isolated structure's total mass, M (i.e., $M = m_b + \sum_{i=1}^{5} m_i$). The isolation damping ratio is selected as 10 percent. The yield strength of the LRB is selected as 0.05W (i.e., W=Mg represents the total weight of the base-isolated structure) and yield displacement as 0.025m. The

Preprints (www.preprints.org) | NOT PEER-REVIEWED | Posted: 15 December 2023 doi:10.20944/preprints202312.1127.v1

normalized inertance, β of the supplemental devices is calculated by considering the total mass, M. The auxiliary stiffness and damping of the optimal TMDI (for the specified value of T_b and ξ_b) are selected corresponding to which minimizes the σ_x^2 of a rigid-base isolated structure under white-noise earthquake excitation using equations (8) and (9). The viscous damping of FID is defined by ξ_f using equation (10) and considering the total mass of the isolated structure, and taken as ξ_f=β/2. The seismic response of the isolated building with supplemental TMDI, ADAS, FID, and FD devices is evaluated numerically by solving the governing equations of motion using the step-by-step method [49].

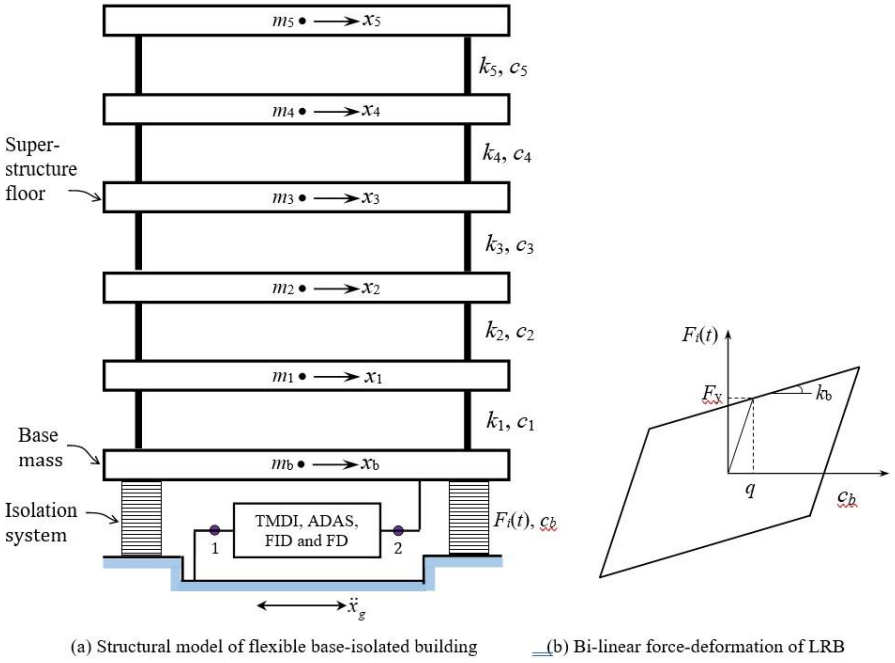

Figure 8. Modelling of the flexible base-isolated building with TMDI, ADAS, FID, and FD and bi-linear characteristics of LRB.

Three real earthquake motions, namely the north-south component of El-Centro, 1940 earthquake, N00E component of the 1989 Loma Prieta earthquake (measured at Los Gatos Presentation Centre), and 270 component of the 1992 Landers earthquake (measured at Lucerne Valley), are selected. The peak ground acceleration (PGA) of El-Centro, Loma Prieta, and Landers earthquake motions are 0.34g, 0.57g, and 0.73g, respectively. The response quantities of interest are the top floor absolute acceleration ($\ddot{x}_5^a$), relative base displacement (x_b), force in the isolation system (F_{is}), force in the supplemental device (F_{sup}), and total base shear (F). The selected force quantities are normalized with W.

The time variation of the top floor absolute acceleration, relative base displacement, the force in the isolation system, the force in the supplemental device, and total base shear are shown in Figure 9. The responses are shown for the Loma Prieta, 1989 earthquake and compared with the corresponding response of isolated structures without supplemental devices (referred to as BIS). The figure indicates that the peak value of the top floor acceleration for BIS+TMDI, BIS+ADAS, and BIS+FD is the same as that of BIS, implying that these supplemental devices are not much altering the top floor acceleration. However, there is an almost 3.61 times increase in the peak top floor acceleration of the isolated structure with FID compared to the corresponding peak acceleration of BIS. This is unacceptable as the FID defeats the primary purpose of seismic isolation by increasing the structural acceleration. It was also noted that the base-isolated structure with FID's absolute acceleration contains high-frequency components, which could be harmful to equipment or a secondary system that is sensitive to high-frequency vibrations. There is a reduction in base

Preprints (www.preprints.org) | NOT PEER-REVIEWED | Posted: 15 December 2023 doi:10.20944/preprints202312.1127.v1

displacement by all the supplemental devices. It was observed to decrease by 23.8 to 32.8 percent compared to the corresponding BIS. The base displacement of isolated structures with ADAS is less than the corresponding TMDI. This is interesting and primarily happens because the peak base displacement occurs in the large initial cycles of the response. By that time, the TMDI is not adequately tuned to dissipate the input seismic energy. However, the TMDI is more effective in reducing the subsequent peak response in comparison to the ADAS. The variation of force in the isolation system is similar to that of the isolator displacement for all supplemental devices. The peak value of the force in the supplemental devices for the isolated structure with FID is almost 3 to 4 times that of other devices. The peak total base shear is reduced for isolated structures with TMDI, ADAS, and FD and immensely increased for the FID compared to the corresponding total base shear of the BIS.

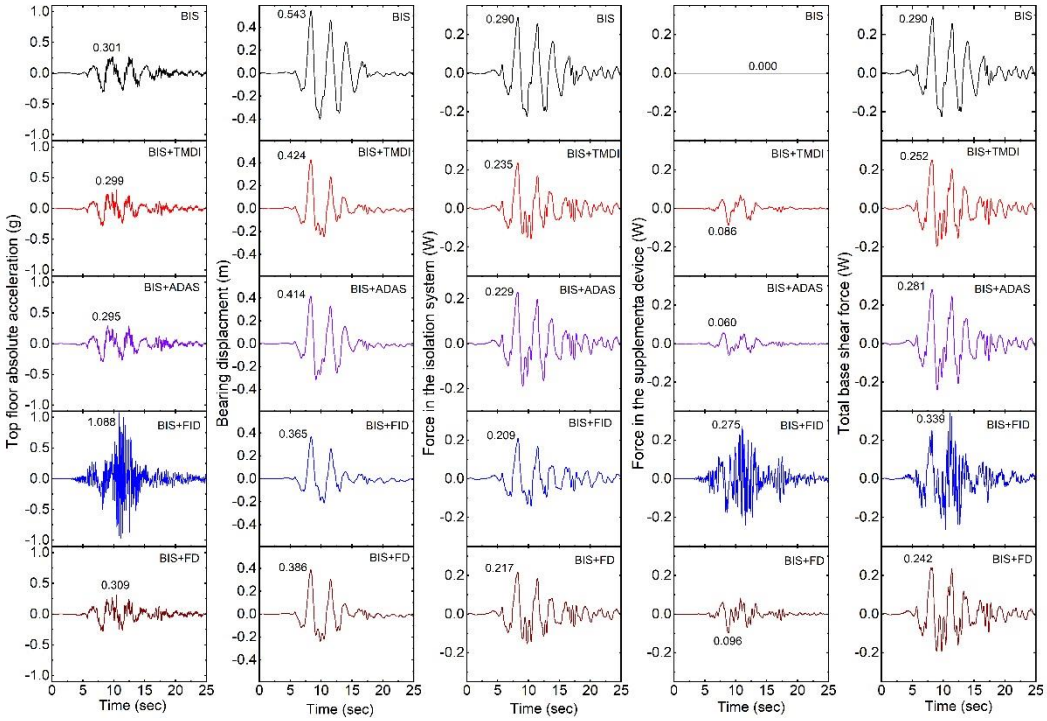

Figure 9. Time history of response of a flexible base-isolated building subjected to the Loma Prieta, 1989 earthquake (T_b = 3 sec and β = 0.4).

The effects of the β on the peak top floor absolute acceleration, relative base displacement, the force in the isolation system, the force in the supplemental device, and the total base shear of the base-isolated structure with different supplemental devices and earthquakes are shown in Figure 10. The figure indicates that the peak top floor acceleration is not very sensitive to β and quite comparable to the base-isolated structures with supplemental TMDI, ADAS, and FD. However, the peak top floor acceleration increases with β for the isolated structure with supplemental FID. This can be explained with the help of Figure 6, which shows that the grounded inerter connected to the base mass will directly transmit the vibration (i.e., accelerations) associated with high-frequency amplitudes in the earthquake ground motion. This confirms that the inerter in the FID has detrimental effects as a supplemental device to the isolation system, increasing the structural accelerations. The peak base displacement of the base-isolated structure with supplemental devices decreases with the increase of β. A comparison of the peak base displacement of the base-isolated structures with TMDI and the corresponding ADAS indicates a greater reduction in the base displacement by ADAS compared to TMDI.

Further, there is a greater reduction in base displacement for the isolated structures with FID than with FD. The variation of peak force in the isolation system has a similar trend to base displacement. The peak force in the supplemental devices increases with the increase in β. However,

Preprints (www.preprints.org) | NOT PEER-REVIEWED | Posted: 15 December 2023 doi:10.20944/preprints202312.1127.v1

the force in the FID is substantially higher in comparison to the force of other supplemental devices. The peak total base shear of isolated structures with TMDI, ADAS, and FD is not very sensitive to the β but it increases for the FID. Thus, it can be concluded that the inerter in the FID increases the structural acceleration as well as the total base shear.

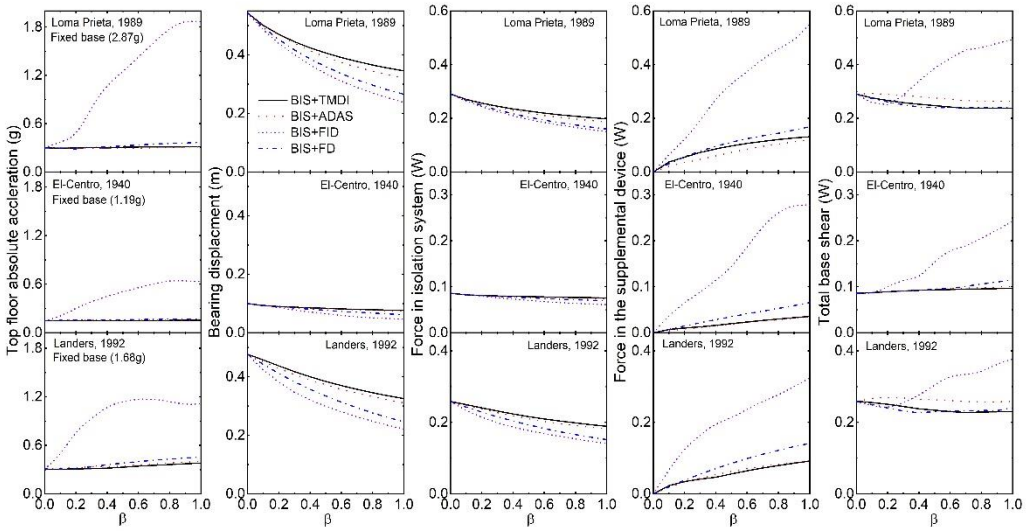

Figure 10. The effects of the β on the peak response of a flexible base-isolated building subjected to various earthquakes (T_b = 3 sec).

The effects of β on the peak top floor absolute acceleration, relative base displacement, the force in the isolation system, the force in the supplemental device, and the total base shear of the base-isolated structures with T_b = 4 sec for different earthquakes are shown in Figure 11. The trends of the results in Figure 11 are similar to those observed in Figure 10 for considering T_b = 3 sec.

Based on the discussion of the presented results, it can be concluded that there is a greater or comparable reduction in the base displacement by corresponding ADAS in comparison to the optimal TMDI. Further, an inerter of the FID attached to the ground and an isolated structure have detrimental effects on seismic isolation by transmitting the vibrations associated with high-frequency accelerations and increasing the base shear. The study's overall conclusion is that inerter-based supplemental devices such as TMDI and FID may not be very effective for the base-isolated structures to warrant their practical application. On the other hand, a pair of inerters with a clutching effect might be able to significantly reduce the displacement in the base-isolated structure's isolation system [50–53]. Also, the performance of the inerter-based dampers in conjunction with negative stiffness devices was somewhat encouraging for the base-isolated structures [54,55]. The current study is primarily concerned with the inerter's function in the recently investigated supplemental dampers for base-isolated structures. However, it is strongly recommended to compare their performance with the widely researched dampers, such as magnetorheological dampers, negative stiffness dampers, semi-active variable friction and stiffness devices, etc. It is also recommended that the findings of the present study be experimentally validated.

Preprints (www.preprints.org) | NOT PEER-REVIEWED | Posted: 15 December 2023 doi:10.20944/preprints202312.1127.v1

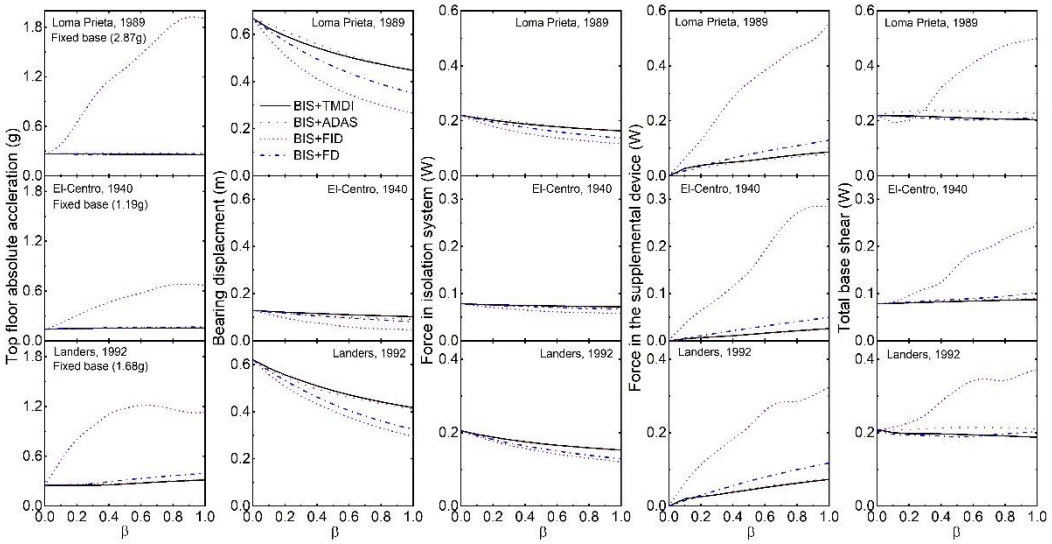

Figure 11. The effects of the β on the peak response of a flexible base-isolated building subjected to various earthquakes (T_b = 4 sec).

6. Conclusions

From this research study of base-isolated structures equipped with inerter-based supplemental devices, the following conclusions can be drawn:

1. The TMDI (especially with a sizeable inertance ratio) may not control the response of the base-isolated structure through tuning effects but controls by the added heavy damping and stiffness of its auxiliary damper under real earthquake excitation. It is recommended that the corresponding damping and stiffness (i.e., ADAS) of the TMDI be installed in parallel to the isolation device for better response control and economy.
2. The variance of base-isolated structures with optimal TMDI subjected to broadband earthquake excitation is higher than the corresponding ADAS for lower values of the inertance ratio. However, for the higher inertance ratio, the ADAS is superior to the TMDI in reducing the displacement variance of the base-isolated structures.
3. For a broadband excitation, the displacement variance of the base-isolated structure with supplemental FID is not influenced by the inerter of the FID. The reduction in displacement is primarily happening due to the added damping of the FID. It is recommended that the FD alone can better control the response of the base-isolated structure as compared to the FID.
4. There is a greater or comparable reduction in the base displacement of the isolated structures under real earthquake excitation by ADAS compared to the corresponding optimal TMDI. It implies that with a suitable ADAS, better control of response in the isolation system can be achieved.
5. The high-frequency components are present in the absolute structural acceleration of a base-isolated structure with FID and may have detrimental effects on high-frequency-sensitive types of equipment or secondary systems. An inerter attached to the ground and an isolated structure defeats the purpose of seismic isolation by transmitting the vibrations and increasing the base shear of the structure.
6. The inerter-based supplemental devices such as TMDI (or TID) and FID (or EIMD) may not be very effective for the base-isolated structures to warrant their practical application.

Funding: This research received no external funding.

Data Availability Statement: Some or all data, models, or code that support the findings of this study are available from the corresponding author upon reasonable request.

Conflicts of Interest: The authors declare no conflict of interest.

References

1. Ma, R.; Bi, K.; Hao, H. Inerter-based structural vibration control: A state-of-the-art review. *Engineering Structures* **2021**, 243, 112655.
2. Smith, M.C. Synthesis of mechanical networks: The inerter. *IEEE Transactions on Automatic Control* **2002**, 47(10), 1648-1662.
3. De Domenico, D.; Ricciardi, G. An enhanced base isolation system equipped with optimal tuned mass damper inerter (TMDI). *Earthquake Engineering and Structural Dynamics* **2018**, 47(5), 1169-1192.
4. De Domenico, D.; Ricciardi, G. Optimal design and seismic performance of tuned mass damper inerter (TMDI) for structures with nonlinear base isolation systems. *Earthquake Engineering and Structural Dynamics* **2018**, 47(12), 2539-2560.
5. De Domenico, D.; Ricciardi, G. Improving the dynamic performance of base-isolated structures via tuned mass damper and inerter devices: A comparative study. *Structural Control and Health Monitoring* **2018**, 25(10), e2234.
6. De Domenico, D.; Impollonia, N.; Ricciardi. G. Soil-dependent optimum design of a new passive vibration control system combining seismic base isolation with tuned inerter damper. *Soil Dynamics and Earthquake Engineering* **2018**, 105, 37-53.
7. De Angelis, M.; Giaralis, A.; Petrini, F.; Pietrosanti, D. Optimal tuning and assessment of inertial dampers with grounded inerter for vibration control of seismically excited base-isolated systems. *Engineering Structures* **2019**, 196, 109250.
8. Di Matteo, A.; Masnata, C.; Pirrotta, A. Simplified analytical solution for the optimal design of Tuned Mass Damper Inerter for base isolated structures. *Mechanical Systems and Signal Processing* **2019**. 134, 106337.
9. Masnata, C.; Di Matteo, A.; Adam, C.; Pirrotta, A. Assessment of the tuned mass damper inerter for seismic response control of base-isolated structures. *Structural Control and Health Monitoring* **2021**, 28, e2665.
10. Li, Y.; Li, S.; Chen, Z. Optimal design and effectiveness evaluation for inerter-based devices on mitigating seismic responses of base isolated structures. *Earthquake Engineering and Engineering Vibration* **2021**, 20, 1021-1032.
11. Chowdhury, S.; Banerjee, A.; Adhikari, S. Enhanced seismic base isolation using inertial amplifiers. *Structures* **2021**, 33, 1340-135.
12. Jangid, R.S. Optimum parameters and performance of tuned mass damper-inerter for base-isolated structures. *Smart Structures and Systems* **2022**, 29(4), 549-560.
13. Han, G.; Wu, Y.; Hou, G.; Yue, Z. Optimal design of nuclear power plants containment with tuned mass damper inerter device for earthquake loadings. *Journal of Mechanical Science and Technology*, **2023**, 37(11), 5607-5621.
14. Li, C., Chang, K.; Cao, L.; Huang, Y. Performance of a nonlinear hybrid base isolation system under the ground motions. *Soil Dynamics and Earthquake Engineering* **2021**, 143, 106589.
15. Cao, L.; Li, C. A high performance hybrid passive base-isolated system. *Structural Control and Health Monitoring* **2022**, 29(3), e2887.
16. Pietrosanti, D.; De Angelis, M.; Giaralis, A. Experimental study and numerical modeling of nonlinear dynamic response of SDOF system equipped with tuned mass damper inerter (TMDI) tested on shaking table under harmonic excitation. *International Journal of Mechanical Sciences* **2020**, 184, 105762.
17. Pietrosanti, D.; De Angelis, M.; Giaralis, A. Experimental seismic performance assessment and numerical modelling of nonlinear inerter vibration absorber (IVA)-equipped base isolated structures tested on shaking table. *Earthquake Engineering and Structural Dynamics* **2021**, 50(10), 2732-2753.
18. Qian, F.; Luo, Y.; Sun, H.; Tai, W.C.; Zuo, L. Optimal tuned inerter dampers for performance enhancement of vibration isolation. *Engineering Structures* **2019**, 198, 109464.
19. Jangid, R.S. Optimum tuned inerter damper for base-isolated structures. *Journal of Vibration Engineering & Technologies* **2021**, 9, 1483-1497.
20. Nyangi, P.; Ye, K. Optimal design of dual isolated structure with supplemental tuned inerter damper based on performance requirements. *Soil Dynamics and Earthquake Engineering* **2021**, 149, 106830.
21. Zhang, L.; Guo, M.; Li, Z.; Zhu L.; Meng Y. Optimal design and seismic performance of base-isolated storage tanks using friction pendulum inerter systems. *Structures* **2022**, 43, 234-248.
22. Huang, X.; Hu, Z.; Liu, Y.; Nie, L. Study on seismic performance of TID-LRB hybrid control system under multi-level earthquakes, *Buildings* **2022**, 12(9), 1465.

23. Li, J.-Y.; Lu, J.; Zhou, H. Reliability analysis of structures with inerter-based isolation layer under stochastic seismic excitations. *Reliability Engineering and System Safety* **2023**, 235, 109222.
24. Tai, Y.-J.; Huang, Z.-W.; Chen, C.; Hua, X.-G.; Chen, Z.-Q. Geometrically nonlinearity analysis and performance evaluation of tuned inerter dampers for multidirectional seismic isolation. *Mechanical Systems and Signal Processing* **2022**, 168, 108681.
25. Stanikzai, M.H.; Elias, S.; Matsagar, V.A.; Jain, A.K. Seismic response control of base-isolated buildings using multiple tuned mass dampers. *The Structural Design of Tall and Special Buildings* **2019**, 28(3), e1576.
26. Stanikzai, M.H.; Elias, S.; Rupakhety, R. Seismic response mitigation of base-isolated buildings. *Applied Sciences* **2020**, 10(4), 1230.
27. Zhao, Z.; Chen, Q.; Zhang, R.; Pan, C.; Jiang, Y. Optimal design of an inerter isolation system considering the soil condition. *Engineering Structures* **2019**, 196, 109324.
28. Zhao, Z.; Zhang, R.; Jiang, Y.; Pan, C. Seismic response mitigation of structures with a friction pendulum inerter system. *Engineering Structures* **2019**, 193, 110-120.
29. Sun, H.; Zuo, L.; Wang, X.; Peng, J.; Wang, W. Exact H2 optimal solutions to inerter-based isolation systems for building structures. *Structural Control and Health Monitoring* **2019**, 26(6), e2357.
30. De Domenico, D.; Deastra, P.; Ricciardi, G.; Sims, N.D.; Wagg, D.J. Novel fluid inerter based tuned mass dampers for optimised structural control of base-isolated buildings. *Journal of the Franklin Institute* **2019**, 356(14), 7626-7649.
31. De Domenico, D.; Ricciardi, G.; Zhang, R. Optimal design and seismic performance of tuned fluid inerter applied to structures with friction pendulum isolators. *Soil Dynamics and Earthquake Engineering* **2020**, 132, 106099.
32. Jiang, Y.; Zhao, Z.; Zhang, R.; De Domenico, D.; Pan, C. Optimal design based on analytical solution for storage tank with inerter isolation system. *Soil Dynamics and Earthquake Engineering* **2020**, 129, 105924.
33. Akhare, A.R. Seismic response control of base-isolated structures with fluid inerter damper. *International Journal of Structural Engineering* **2023**, 13(1), 1-21.
34. Zhao, Z.; Hu, X.; Zhang, R.; Xie, M.; Liu, S. Advantages and design of inerters for isolated storage tanks incorporating soil conditions. *Thin-Walled Structures* **2024**, 195, 111356.
35. Wang, H.; Shen, W.; Li, Y.; Zhu, H.; Zhu, S. Dynamic behavior and seismic performance of base-isolated structures with electromagnetic inertial mass dampers: Analytical solutions and simulations. *Engineering Structures* **2021**, 246, 113072.
36. Lin, G.-L.; Lin, C.-C.; Li, Y.-H.; Lin, T.-T. Theoretical and experimental analysis of an electromagnetic seismic isolation system. *Engineering Structures* **2022**, 250, 113411.
37. Villaverde R. Reduction in seismic response with heavily-damped vibration absorbers. *Earthquake Engineering and Structural Dynamics* **1985**, 13, 33-42.
38. Bakre, S.V.; Jangid, R.S. Optimum parameters of tuned mass damper for damped main system. *Structural Control and Health Monitoring* **2007**, 14(3), 448-470.
39. Pietrosanti, D.; De Angelis, M.; Basili, M. Optimal design and performance evaluation of systems with Tuned Mass Damper Inerter (TMDI). *Earthquake Engineering and Structural Dynamics* **2017**, 46, 1367-1388.
40. Prakash, S.; Jangid, R.S. Optimum parameters of tuned mass damper-inerter for damped structure under seismic excitation *International Journal of Dynamics and Control* **2022**, 10(5), 1322-1336.
41. Makris, N. Rigidity - plasticity - viscosity: Can electrorheological dampers protect base-isolated structures from near-source ground motions? *Earthquake Engineering and Structural Dynamics* **1997**, 26(5), 571-591.
42. Swift, S.J.; Smith, M.C.; Glover, A.R.; Papageorgiou, C.; Gartner, B.; Houghton, N.E. Design and modelling of a fluid inerter. *International Journal of Control* **2013**, 86(11), 2035-2051.
43. Liu, X.; Jiang, J.Z.; Titurus, B.; Harrison, A. Model identification methodology for fluid-based inerters. *Mechanical Systems and Signal Processing* **2018**, 106, 479-494.
44. Wagg, D.J.; Pei, J.-S. Modeling a helical fluid inerter system with time-invariant mem-models. *Structural Control and Health Monitoring* **2020**, 27, e2579.
45. Roberts, J.B.; Spanos, P.D. *Random vibration and statistical linearization*. Chichester, UK, Wiley, **1990**.
46. Kanai, K. Semi-empirical formula for the seismic characteristics of the ground. *Bulletin of the Earthquake Research Institute* **1957**, 35(2), 309-325.
47. Tajimi, H. A statistical method of determining the maximum response of a building structure during an earthquake. *Proc. of 2nd World Conference on Earthquake Engineering* **1960**, 11, 781-798.
48. Kelly, J.M. *Earthquake-resistant design with rubber*, 2nd Ed. London: Springer-Verlag, **1997**.

49. Chopra, A.K. *Dynamics of Structures: Theory and Applications to Earthquake Engineering*. 5th Edn.; Pearson, NJ, **2017**.
50. Li, L.; Liang, Q. Effect of inerter for seismic mitigation comparing with base isolation. *Structural Control and Health Monitoring* **2019**, 26(10), e2409.
51. Makris, N.; Moghimi, G. Displacements and forces in structures with inerters when subjected to earthquakes. *Journal of Structural Engineering* **2019**, 145(2), 04018260.
52. Jangid, R.S. Seismic performance of supplemental inerter and spring with on-off effects for base-isolated structures. *Journal of Infrastructure Intelligence and Resilience* **2023**, 2(2), 100038.
53. Jangid, R.S. Seismic performance of a clutched inerter for structures with curved surface sliders. Structures **2023**, 49, 44-57.
54. Gao, H.; Xing, C.; Wang, H.; Li, J.; Zhang, Y. Performance improvement and demand-oriented optimum design of the tuned negative stiffness inerter damper for base-isolated structures. *Journal of Building Engineering* **2023**, 63, 105488.
55. Islam, N.U.; Jangid, R.S. Optimum parameters and performance of negative stiffness and inerter based dampers for base-isolated structures. *Bulletin of Earthquake Engineering*. **2023**, 21(3), 1411-1438.